Investigating on Structural, Optical, Magnetic and Photocatalytic Activities of ZnS and Co^{2+}: ZnS NPs Synthesized by Hydrothermal Process Under MeB Dye

S. Upputuri
Presidency College
S. Lakshmanan
Bharath University
Ramalakshmi N (nramalakshmi453@gmial.com)
Presidency College
S. Arul Antony
Presidency College

Research Article

Keywords: Co2+, ZnS, Hydrothermal, Physico-Chemical, Photocatalytic, MeB

Posted Date: September 7th, 2021

DOI: https://doi.org/10.21203/rs.3.rs-866114/v1

Abstract

In present work, the structural, morphological, optical and photocatalytic activities of ZnS and Co^{2+}: ZnS NPs were prepared through chemical route as hydrothermal process at room temperature. ZnS and Co^{2+}: ZnS were characterized by using various techniques such as, XRD, SEM-EDX, TEM-SAED, UV-visible, PL and BET. The spherical-like morphology with the average crystallite size was found to be 8 to 15 nm. Among them results, it showed that the Co^{2+} atoms were incorporated into the ZnS lattice, forming cubic phase as the Co^{2+} dopant concentration increases from 0 to 2 %. The band gap energy of the ZnS and Co^{2+}: ZnS increases from 3.5 to 4.10 eV, which enables stronger absorption of UV region. During catalytic process, Co^{2+} act as electron trapping center, which inhibits the recombination of the photo induced holes and electrons as showed higher degradation efficiency for MeB.

1. Introduction

In semiconductor, the nanostructured materials are strongly attracted more interest in physics, chemistry, catalytic, material science and biology, due to size tuned optical and unique properties. Recent years, the semiconductor based photocatalytic technique has been attracted significant awareness in the fields of environmental remediation [1–2]. It showed ease separation of the catalyst from the reaction products of heterogeneous photo catalyst. During process, the electrons and holes undergo redox reactions present in the RhB dye solution, which is used to remove waste waters, involving the degradation of less toxic semiconductor materials. The various approaches have been used to enhance the charge separation with improved their efficiency of photo catalyst such as, elemental doping, coupling two semiconductors and so on [2–3]. Among them, the photocatalytic technique has a wider range advantages compared to traditional techniques in waste water treatment and it is used for industrial applications. ZnS is a II-VI semiconductor with the direct band gap of 3.68 eV. Recently, ZnS showed prominent applications like solar cells, LED, optoelectronic and so on that require an appropriate particle size, size distribution and methods. In past decades, the promising results were achieved by using various metal dopants such as Mg, Co, Mn, Ni and Cd. Among them, Co^{2+} ions as dopant improve the visible light absorption capacity of catalyst owing to their 3d transition and their potential properties [6–10]. Up to now, there are several methods employed for the synthesis of various metal ions-doped ZnS nanoparticles such as, wet-chemical, combustion process, microwave assisted method and so on. Among them, the hydrothermal process are uniquely provides efficient, nucleation, high purity, easy manipulation and producing small particles [11–12]. In the present paper, undoped and Co^{2+}-doped ZnS nanoparticles were synthesized and its structural, morphological, optical properties were discussed. Further, the photocatalytic activities of undoped and Co^{2+}-doped ZnS on MeB under UV radiation were studied. From these findings, Co^{2+}-doped ZnS ions are modifying the various properties and its photocatalytic mechanism was also investigated.

2. Experimental

2.1 Chemicals and Materials

In this work, all the chemicals were purchased from Merck. Zinc acetate dehydrates ($ZnAC_2.2H_2O$), double distilled water, NH_3 and Thiourea (CH_4N_2S) were used as the starting materials for preparing the ZnS nanoparticles. Then, Cobalt acetate dehydrates ($CoAC_2.2H_2O$) were used as dopant for covering the ZnS nanoparticles.

2.2 Preparation of ZnS nanoparticles

Present work, 0.1 M of $ZnAC_2.2H_2O$ and 0.3 M of CH_4N_2S were dissolved in double distilled water under continuous stirring for 2 hrs. Then, the ammonia solution was added to drop wise due to well control for chemical homogeneity under acetic pH condition. This mixed solution was taken in an autoclave and kept at 180 ^{0}C for 12 hrs in a muffle furnace that, they were cooled to room temperature. Finally, the obtained sample was filtered and dried at 120 ^{0}C for 6 hrs in a vacuum.

2.3 Preparation of Co^{2+}: ZnS nanoparticles

Among them, the same procedure was adopted to preparation of Co^{2+}: ZnS particles in the nanosized range using 0.01 M of $CoAC_2.2H^2O$ as dopant (2% and 3%).

2.4 Characterizations

The crystalline structure was carried out by powder X-ray diffraction in a Bruker D8 Advance using monochromatized Cu kα radiation as λ = 0.15496 nm. SEM-EDX was performed with a S4800 field emission SEM at an accelerating voltage of 5 kV. From TEM-SAED instrument, the morphology and particle size were analyzed using a TEM Philips model CM 20 operated at an accelerating voltage of 200 kV. UV-visible and PL were collected using a Varian Cary 5E UV-vis Spectrophotometer and Jobin Yvan Flourometer. From BET instrument, the N_2 adsorption measurements were done on a Micromerities ASAP 2010 physisorption apparatus.

2.5 Photocatalytic Experiment

The photocatalytic activity of synthesized samples was tested by the degradation of MeB under UV light irradiation of 365 nm. Present work, 40 mg photo catalyst was suspended in MeB solution. Then, the mixed solution was oscillated in darkness 6 h. after reaching adsorption equilibrium, the photo catalyst reaction was initiated by irradiation the system with a 350 w xenon lamp. At given time intervals, 4ml aliquots were collected centrifuged and then filtered to remove the catalyst particles for analysis. The filtrates were finally analyzed using a UV-visible spectrophotometer UV-2450. Hence, the degradation efficiency (□) was calculated by using □ ——— with the C_o before illumination (concentration of the MeB) and C_t after certain irradiation at a time (t) (concentration of the MeB).

3. Result And Discussion

Figure 1 (a-c) shows the XRD patterns of ZnS and Co^{2+}: ZnS NPs. The observed XRD peaks corresponding to three indexed planes such as, (111), (220) and (311) with the other phase peaks were

not observed due to impurities, to confirm the formation of cubic structure (JCPDS. NO. # 05-0566) [13]. By using Debye-Scherer's, the average crystalline sizes were found to be 3.7, 3.2 and 2.9 nm, respectively [14–15]. From XRD, the obtained diffraction peaks are decreases with the increase of dopant concentration as Co^{2+}, it's indicate a smaller crystallite size with low crystallinity due to lattice distortions [15–16]. Since, the ionic radius of Co^{2+} (0.65 nm) is slightly less than that of the Zn^{2+} (0.74 nm) ion and the lattice parameters (a = 5.386Å) of Co^{2+}: ZnS sample are slightly less than the ZnS (a = 5.391 Å) [16–17]. Finally, the XRD peaks of Co^{2+}: ZnS (3%) are broader than that of other samples, its showed smaller size of the particles.

Figure 2 (a-f) shows the SEM-EDX of ZnS and Co^{2+}: ZnS NPs. The spherical-like morphology was observed with the compositional elements were presented, such as cobalt, sulfur and zinc. The cobalt ions are equally distributed in the ZnS lattice with the extra peaks was not present, its high purity [15–18]. Figure 3 (a-c) shows the TEM image of ZnS and Co^{2+}: ZnS NPs. The particle sizes were found to be 3.7, 3.2 and 2.9 nm, respectively. Co^{2+}: ZnS particles have a smaller size than the ZnS particles. These dots and rings are clearly indicating that the synthesized samples has cubic structure and there was no structural change, this was due to cobalt doping in the ZnS system, its indicates high purity [18–20].

Figure 4 (a-c) shows the UV-Visible of ZnS and Co^{2+}: ZnS NPs. The synthesized samples were occurred in the UV region, its indicate blue shift compared to bulk ZnS due to the quantum confinement effect. By applying the value of n = ½, the observed band gap are calculated as 3.66, 3.89 and 4.10 eV, respectively. It is concluded, 3% of Co^{2+}: ZnS particle have higher optical band gap compared to other samples due to smaller particle size. Consequently, the increased optical band gap materials suggest that the synthesized nanoparticles influence in the optical devices based applications, it can be tuned by adding the dopant as Co^{2+} [19–23]. Figure 5 (a-c) shows PL spectra of ZnS and Co^{2+}: ZnS NPs with a excitation wavelength of 350 nm. The emissions were observed at 445 nm due to recombination of sulfur vacancy defects as internal vacancy of zinc (holes trapped) and sulfur (donor level) atom. Since, the emission spectra were observed in blue shift compared to bulk counterparts and it is useful for optoelectronic devices [22–24, 12].

Figure 6 (a-b) shows the photocatalytic activity of undoped and Co^{2+}: ZnS. The characteristic absorption peak was observed at 645 nm at various time intervals upto 120 min. It's corresponding to the absorption intensity slightly decreased as well as irradiation time increased with their new absorption bands is not present due to impurities. In pure ZnS, the photo generation rate of holes and electrons is much faster than separation rate; it's producing low carrier separation efficiency. In Co^{2+}: ZnS, the photo-electrons preferentially transfer to the doping level due to Co^{2+} atoms in the ZnS. It's providing the electron trapping centers and recombination of holes and electrons, resulting in the increase of the carrier separation efficiency. Among them, Co^{2+}: ZnS catalyst has a large surface area, small grain size and catalytic activity is higher than that of undoped ZnS catalyst. Figure 7 (a-b) shows the degradation efficiency of undoped and Co^{2+}: ZnS catalyst. The degradation efficiency was found to be and 60 and 93.22 %, respectively. Among these values, Co^{2+}: ZnS particles are enhanced to the higher photocatalytic activity

due to enhancement of the energy transfer. During process, Co^{2+} doped ions inserts various localized energy states in the forbidden energy gap as recombination and charge carrier trapping on the surface charge transfer and it's indicate that the Co^{2+} ions are provided extra energy level with reduced bandgap due to smaller size of particles in the ZnS lattice.

Table 1 gives the degradation of absence and presence of Co^{2+}: ZnS catalyst using MeB under UV light irradiation. A blank experiment was found to be 0.31 x 10^{-3}. During synthesis, 2 % of Co^{2+}: ZnS catalyst was found to be 1.87 x 10^{-3} and 4.43 x 10^{-3} and 3 % of Co^{2+}: ZnS catalyst was found to be 2.33 x 10^{-3} and 6.36 x 10^{-3}, respectively. It concluded that the 3 % of Co^{2+}: ZnS catalyst has strong efficiency of degradation. Total Organic Carbon (TOC) analysis of the Co^{2+}: ZnS catalyst in the presence of MeB dye was performed under UV light irradiation as shown in Fig. 11 (a-c). In TOC images, Co^{2+}: ZnS catalyst of TOC removal was found to be 10.24, 72.18 and 88.23 % after 120 min of irradiation. Among these results, it's indicates that the color disappearance of the MeB dye was faster than the degree of mineralization. During process, the quick disappearance was arising from the cleavage of the MeB dye bond and their minimal interaction with aliphatic chains. After 120 min, MeB dye molecules were converted to other intermediate forms, which exist in the solution irrespective of the dye de-colorization lead to complete mineralization beyond 120 min. Table 2 gives the COD values of initial and final treated of Co^{2+}: ZnS catalyst under MeB. It is used to measure the amount of organic components in terms of the total amount of O_2 required to oxidize it to CO_2 and H_2O via dichromate reflux method. In table 2, the synthesized catalyst has high potential for the removal of MeB due to decreased COD values. Consequently, TOC and COD results showed that the 3% of Co^{2+}: ZnS catalyst has higher photocatalytic activities than the other samples. In addition, the detailed drgradation mechanism of undoped and Co^{2+}: ZnS catalyst can be summerized below.

$$Co - ZnS + h\gamma \rightarrow Ce - ZnS\ (e^-_{CB} + h^+_{VB})$$

$$e^-_{CB} + O_2 \rightarrow O_2^{\cdot -}$$

$$h^+_{VB} + H_2O \rightarrow OH^{\cdot} + H^+$$

$$O_2^{\cdot -} + H^+ \rightarrow HO_2^{\cdot}$$

$$O_2^{\cdot -} + H_2O \rightarrow HO_2^{\cdot} + OH^-$$

$$HO_2^{\cdot} + H_2O \rightarrow H_2O_2 + OH^-$$

$$H_2O_2 \rightarrow 2OH^{\cdot}$$

$$h_{VB}^+ + H_2O \rightarrow H^{\cdot} + .OH$$

$$h_{VB}^+ + OH^- \rightarrow {\cdot}OH$$

$$OH^{\cdot} + MB \rightarrow \text{Degraded product } (CO_2 \uparrow + H_2O)$$

BET images of ZnS and Co^{2+}: ZnS NPs with the N_2 adsorption-desorption isotherms as shown in Fig. 10 (a-c). The surface area and pore volume of synthesized samples were calculated as 97, 112 and 148 m^2g^{-1} and 0.25, 0.34 and 0.63 cm^3g^{-1}, respectively. Its corresponds to pore size distribution at ~(12–15), (9–13) and (5–9) nm, respectively. Since, the surface area of ZnS samples gradually increases with the increase of cobalt ions concentration due to smaller particle size. It is concluded that the synthesized samples was composed of many fine crystallites [27, 30].

Figure 11 shows the magnetic properties of 3% doped Co^{2+}: ZnS with the applied magnetic field from −20 to 20 K Oe at room temperature. The prepared ZnS nanoparticles favor the ferromagnetic behavior that reflect low magnetic moment and high coercivity value due to smaller particle size. Further, present case, the coercivity (Hc) of 223 Oe and the saturation magnetic moment of (Ms) 0.00025 (emu/g), respectively. As a result, a low value of saturation magnetic moment and higher value of coercivity were obtained for the 3% Co^{2+}: ZnS sample compared with bulk ZnS [28]. In ferromagnetism, the cubic structure was not changed due to substitution of Co^{2+} ions in the Zn^{2+} surface and it would be very useful for spintronic devices [29, 31].

4. Conclusions

In summary, spherical-like of ZnS and Co^{2+}: ZnS NPs were successfully synthesized by hydrothermal process under different concentration of cobalt ions by hydrothermal process. XRD and TEM studies indicate that the Co^{2+} ions were incorporated into the ZnS lattice, forming the cubic phase. The absorption spectra of ZnS and Co^{2+}: ZnS NPs were exhibit blue shift ensure the quantum confinement effect compared to bulk ZnS due to smaller size of particles. ZnS and Co^{2+}: ZnS NPs improves the photo degradation efficiency using MeB under UV light irradiation. The ferromagnetic behavior was observed from the VSM study. Therefore, the advantages of hydrothermal method for the synthesized nanoparticles permit large-scale production, easy manipulation, low cost.

References

1. R. C. Somersa, P. T. Sneeb, M. G. Bawendia, D. G. Noceraa, *J. Photochem. Photobio. A: Chem.* 248 (2012) 24–29.
2. T.Y Ding, M-S Wang, S.P Guo, G.C Guo, J.S Huang, *Mater. Lett.* 62 (2008) 4529–4531.
3. X. Yu, J. Yu, B. Cheng, B. Huang, *Chem. Eur. J.* 15 (2009) 6731– 6739.
4. Q. I. Rahman, M. Ahmad, S. K. Misra, M. Lohani, *Mater. Lett.* 91 (2013) 170–174.
5. H. R. Pouretedala, A Norozib, M. H. Keshavarza, A. Semnanic, *J. Hazar. Mater.* 162 (2009) 674–681.
6. W. Wang, W. Zhu, H. Xu, *J. Phys. Chem. C*, 112 (2008) 16754–16758.
7. R.Y. Hong, J.H. Li, L.L. Chen, D.Q. Liu, H.Z. Li, Y. Zheng, J. Ding, *Pow. Tech.* 189 (2009) 426–432.
8. M. Saranya, R. Ramachandran, E. J. Samuel, S. K. Jeong, A. N. Grace, *Pow. Tech.* 279 (2015) 209–220.

9. Q. Z Zhai, T-S Jiang, W. H Hu, X Guan, W. Wang, S. Qiu, *Mater. Resea. Bull.* 37 (2002) 1837–1842.
10. B Poornaprakash, U Chalapathi, M Reddeppa, S-H Park, *Super. Micro.* 97 (2016) 104–109.
11. M. E. Pacheco, C. B. Castells, L. Bruzzone, *Sen. Actu. B: Che.* 238 (2017) 660–666.
12. Y. Ding, L. Sun, Y. Jiang, S. Liu, M. Chen, Y. Ding, Q. Liu, *Mater. Sci. Eng. C* 67 (2016) 188–194.
13. F. Ongul, U. Ulutas, S. A. Yuksel, S. S. Yesilkaya, S. Gunes, *Syn. Met.* 220 (2016) 1–7.
14. P. Sajan, R. Vinod, M. J. Bushiri, *J. Lumin.* 158 (2015) 110–115.
15. G. S. Lotey, Z. Jindal, V. Singhi, N. K. Verma, *Mater. Sci. Semi. Proc.* 16 (2013) 2044–2050.
16. S. Ummartyotin, N. Bunnak, J. Juntaro, M. Sain, H. Manuspiya, *Sol. Sta. Sci.* 14 (2012) 299–304.
17. A. I. Cadiş, L. E. Muresan, I. Perhaiţa, E. J. Popovici, L. B. Tudoran, E. Indrea, *Mater. Rese. Bull.* 84 (2016) 57–64.
18. S. Sain, A. Kar, M. Mukherjee, D. Das, S. K. Pradhan, *Adv. Pow. Tech.* 27 (2016) 1790–1799.
19. S. Martínez-Martínez, S. A. Mayén-Hernández, F-D Moure-Flores, M. C. Arenas-Arrocena, E. Campos-González, M. A. Zamora-Antuñano, V. M. Arellano-Badillo, J. Santos-Cruz, *Vacuum* 130 (2016) 154–158.
20. R. Viswanath, H. S. Bhojya Naik, G. S. Yashavanth Kumar, P. N. Prashanth Kumar, K. N. Harish,. M. C. Prabhakara, *Spectrochimica Acta Part A: Mole. Biomol. Spect.* 125 (2014) 222–227.
21. B. Dong, L. Cao, G. Su, W. Liu, H. Qu, H. Zhai, *J. All. Comp.* 492 (2010) 363–367.
22. M. Salavati-Niasari, F. Davar, M. Mazaher, *J. All. Comp*. 470 (2009) 502–506.
23. L. Yue, S. Qi, J. Wang, J. Cai, B. Xin, *Mater. Sci. Semicon. Proc.* 56 (2016) 115–118.
24. B. Poornaprakash, U. Chalapathi, M. Reddeppa, S-H Park, *Super. Micro.* 6036 (2016) 30265–30268.
25. S. Lee, et al. *Mater. Lett.* 58 (2004) 342–346.
26. D. Zhang, G. Li, H. Li. Y. Lu, Chem. *Asian J.* 8 (2013) 26–40.
27. J. Yang, D. Wang, H. Hau, C. Li, *Acc. Chem. Res.* 46 (2013) 1900–1909.
28. R. Chauhan, A. Kumar, R. P. Chaudhary, *J. Lumin.* 145 (2014) 6–12.
29. R. Chauhan, A. Kumar, R. P. Chaudhary, *Spectrochim Acta. A* 113 (2013) 250–256.
30. W. Choi, A. Termin, M. R. Hoffman, *J. Phys. Chem.* 98 (1994) 13669–13679.
31. Q. Xiao, Z. Si, J. Zhang, C. Xiao, X. Tan, *J. Hazard. Mater.* 150. (2008) 62–67.

Tables

Table.1 Photo degradation data of absence and presence of ZnS and Co^{2+}: ZnS NPs

Dye Concentration (ppm)	Mixtures		ZnS	Co^{2+}: ZnS	Degradation efficiency (%)		Reaction rate constant after 150 min (min^{-1})x10^{-3}
	ZnS	Co^{2+}: ZnS			ZnS	Co^{2+}: ZnS	
Initial	Blank		0	0	12	32	0.31
30	0	1	100	0	29	52	2.45
60	1	1	65	69	44	66	3.35
90	2	2	56	55	49	76	4.33
120	1	1	24	70	56	80	5.67
150	1	0	0	100	60	91	6.45

Table.2 COD values of initial and final treated of ZnS and Co^{2+}: ZnS NPs

Dye Concentration (ppm)	Initial COD (mg/L)	Final COD (mg/L)		Photo degradation Efficiency (%)	
		ZnS	Co^{2+}: ZnS	ZnS	Co^{2+}: ZnS
Initial	30.55	13.54	8.27	12.34	23.45
10	74.44	9.44	4.12	22.45	39.33
20	133.54	43.45	15.78	35.67	56.45
30	210.43	64.56	29.56	46.22	69.37
40	290.33	77.44	41.33	51.78	81.86
50	399.34	83.31	52.33	62.66	91.28

Figures

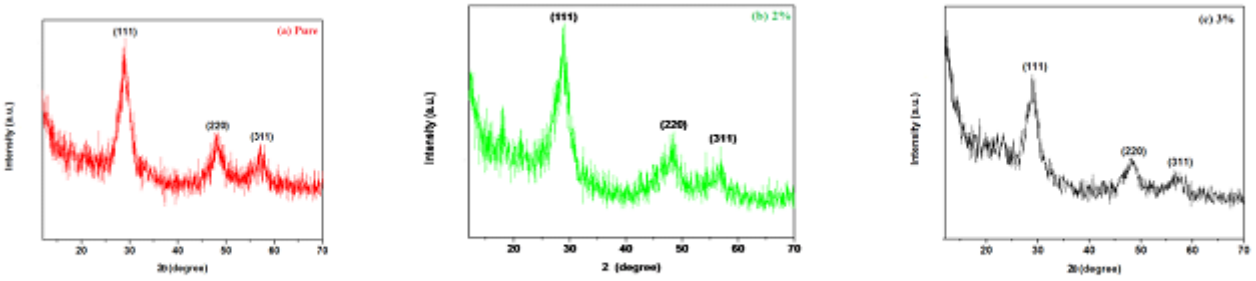

Figure 1

(a-c) shows the XRD patterns of the zinc sulfide samples.

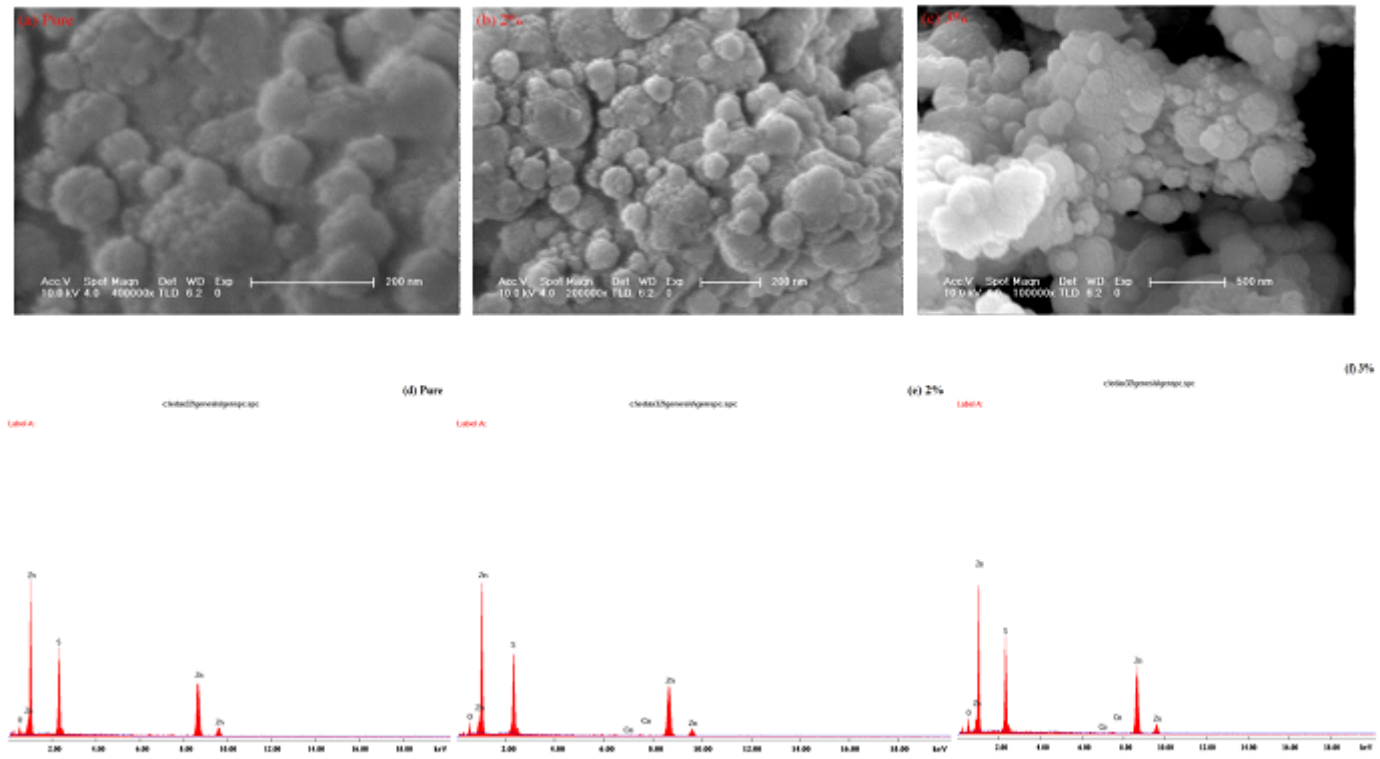

Figure 2

(a-f) shows the SEM-EDX images of the zinc sulfide samples.

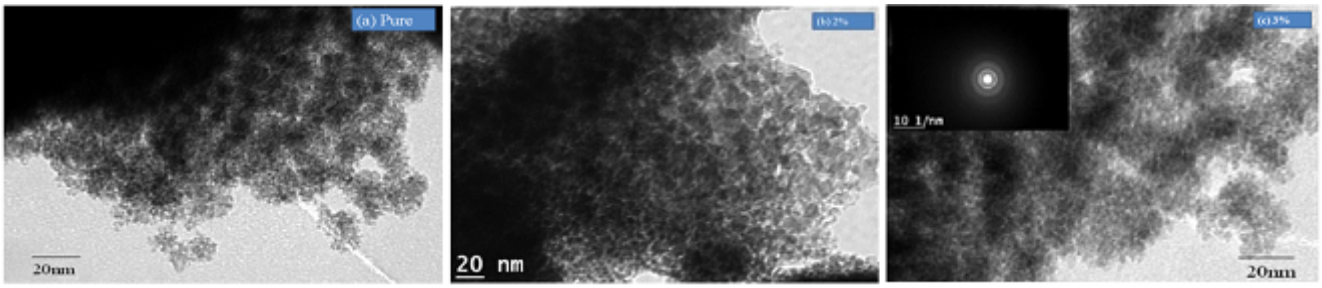

Figure 3

(a-c) shows the TEM-SAED pattern of the zinc sulfide samples.

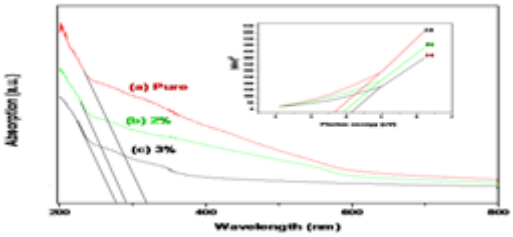

Figure 4

(a-c) shows the UV-Visible spectra of the zinc sulfide samples.

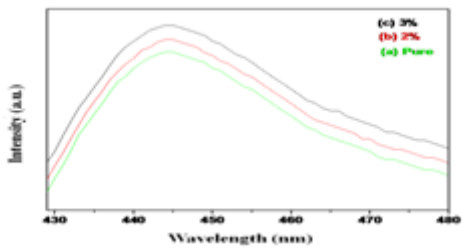

Figure 5

(a-c) shows the PL spectra of the zinc sulfide samples.

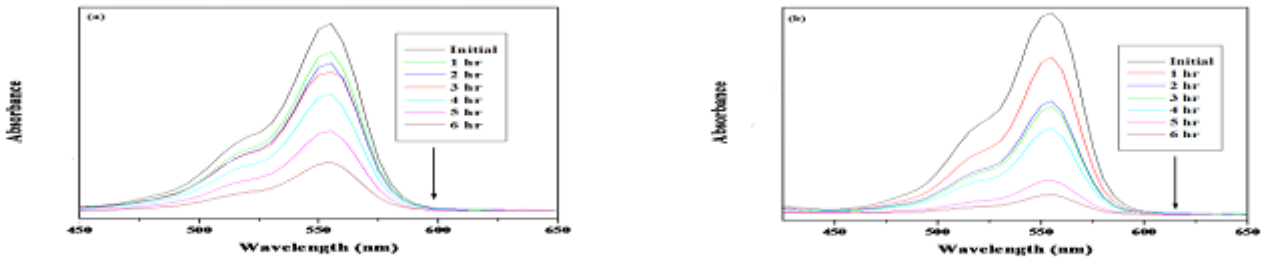

Figure 6

(a-b) shows the Photo degradation of the zinc sulfide samples.

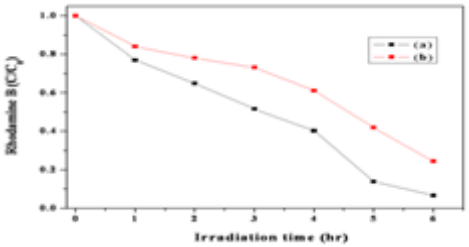

Figure 7

(a-b) shows the Time course concentration of the zinc sulfide samples.

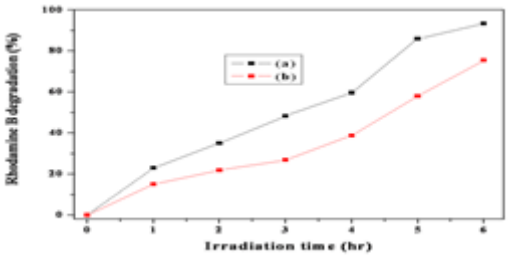

Figure 8

(a-b) shows the Degradation percentage (%) of the zinc sulfide samples.

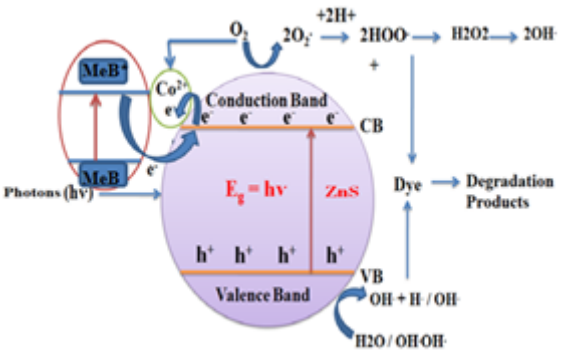

Figure 9

shows the Schematic diagram of catalytic process of the zinc sulfide samples.

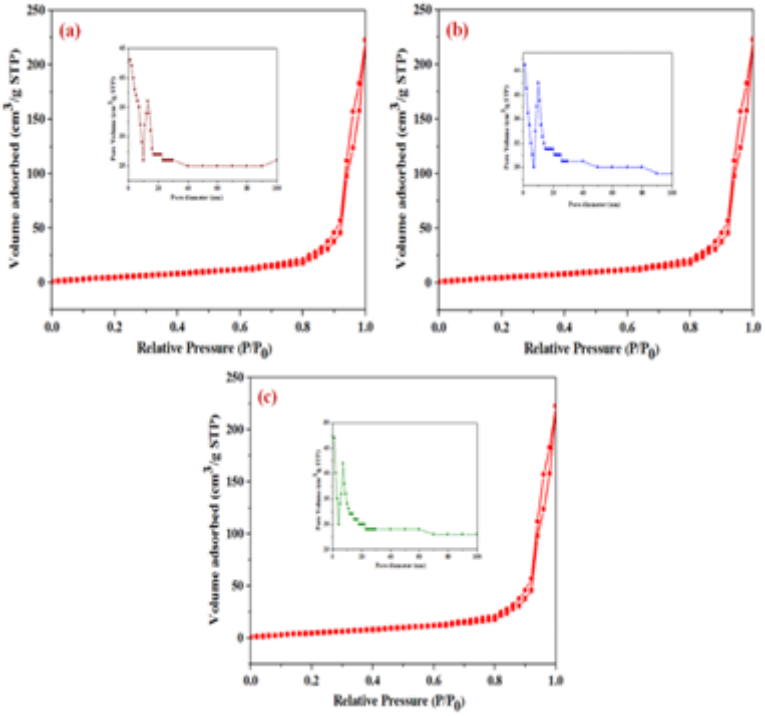

Figure 10

shows the BET of zinc sulfide samples.

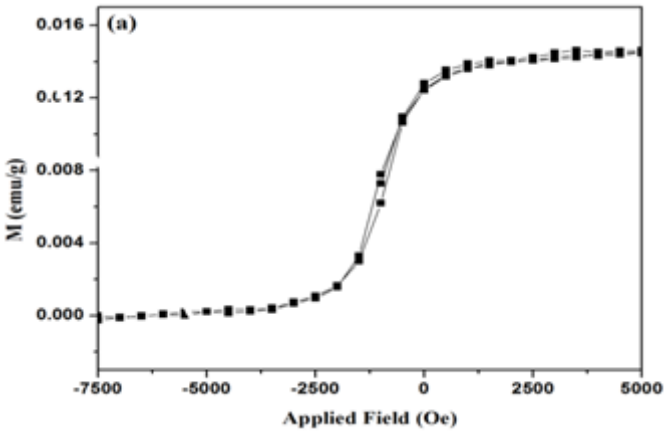

Figure 11

shows the VSM of the zinc sulfide samples.

Supplementary Files

This is a list of supplementary files associated with this preprint. Click to download.

- SupportingMaterials.doc